M. Holzmann, B. Vlach*, and J. Man**

The Ductile-to-Brittle Transition of a Pressure Vessel Steel Embrittled by Step Cooling Heat Treatment

REFERENCE Holzmann, M., Vlach, B., and Man, J., **The ductile-to-brittle transition of a pressure vessel steel embrittled by step cooling heat treatment**, *Defect Assessment in Components – Fundamentals and Applications*, ESIS/EGF9 (Edited by J. G. Blauel and K.-H. Schwalbe) 1991, Mechanical Engineering Publications, London, pp. 569–585.

ABSTRACT The influence of step cooling heat treatment (SCHT) on the embrittlement of 2.25Cr–1Mo pressure vessel steel was studied. Tensile properties, Charpy 'V'-notch fracture behaviour, fracture toughness, and critical tensile stress for brittle fracture initiation were measured in both unembrittled and embrittled (after SCHT) materials. Variation in yield stress and ultimate tensile stress with temperature was not influenced by SCHT; only a significant decrease in fracture stress at liquid nitrogen temperature can be observed after SCHT. The ductile-to-brittle transition temperature of Charpy specimens was shifted after SCHT by 30°C. The use of Weibull statistics for the assessment of critical tensile stresses for brittle fracture initiation showed that this material constant in the as-received state obeys very well two parameter cumulative distribution function. After SCHT, however, double population in a set of measured values was found. One set had the same values of stress as in the as-received state, while the other displayed much lower values. In this set a mixed-mode fracture mechanism of intergranular cracking with the transgranular cleavage was found using a scanning electron microscope. These results proved the heterogeneous character of segregation processes during SCHT.

The median and lower bound fracture toughness temperature curves for unstable brittle initiated fracture were shifted towards higher temperatures due to SCHT. The transition temperature below which this fracture mode occurred was not influenced by SCHT.

Introduction

Various components in power generating plants and chemical plants produced from low alloy steels and operating in the critical temperature range from 350°C to 550°C may become embrittled during their service life **(1)–(4)**. This brittle behaviour manifests itself as an increase in the notch bar ductile-to-brittle fracture appearance transition temperature (FATT) and as a decrease in the toughness of these steels.

Long term temperature ageing tests **(7)–(11)** or accelerated heat treatment procedures known as step cooling heat treatment (SCHT) **(12)** are the methods used to produce embrittlement and thus make it possible to study changes in microstructure, in mechanical properties and the susceptibility of a given steel to embrittlement.

Whilst earlier investigations were concerned mainly with temper embrittlement of Cr–Ni, and Cr–Ni–Mo steels for rotor forgings **(5)–(7)**, recent papers have been concentrated on the study of this phenomenon in Mn–Ni–Mo, Cr–Mo and Cr–Mo–V pressure vessel steels (e.g., **(11)(12)**). Many papers

* Institute of Physical Metallurgy, CAS, Brno, Czechoslovakia.

were concerned with 2.25Cr–1Mo steel. The degree of embrittlement of this particular steel was assessed predominantly by the shift in of FATT **(17)(19)**. Much less is known about the shifting of the fracture toughness/temperature dependence **(20)** and there are practically no data concerning the variation in the critical tensile stress due to embrittlement.

The subject of this paper is the investigation of the influence of SCHT on tensile properties, the transition behaviour of Charpy and fracture toughness test specimens and the critical tensile stress for brittle fracture initiation of 2.25Cr–1Mo steel.

Material, experimental method

A commercially produced plate with dimensions of 12 m × 1 m × 0.08 m was used to make blanks. The heat treatment of the plate (austenitizing 940°C, air cooling, tempering 720°C, air cooling) was carried out by the supplier. The chemical composition (weight percent) was as follows:

C	*Mn*	*Si*	*Cr*	*Mo*	*Ni*	*P*	*S*	*V*	*Cu*	*W*	*Sn*	*Sb*	*As*	*Al*
0.14	0.55	0.25	2.38	0.95	0.35	0.018	0.009	0.01	0.08	0.01	0.008	0.009	0.012	0.015

This results in a Watanabe embrittlement factor (J) for Cr–Mo steel **(27)** ($J = (\mathrm{Mn} + \mathrm{Si})(\mathrm{P} + \mathrm{Sn}).10^4$) of 208. The resulting microstructure was one of tempered bainite. Blanks 30 mm thick, 55 mm wide, and 270 mm long were taken from the middle part of the plate thickness. One set of the blanks was kept in the as-received condition, the other being heat treated by SCHT of the type SOCAL [Grosse-Woerdemann and Dittrich **(12)**]. The following specimens were made from both sets of blanks:

- cylindrical specimens for tensile testing with a diameter of 6 mm and a gauge length of 30 mm;
- Charpy 'V' notch specimens for standard and instrumented impact tests and for static testing;
- single edge notch bend specimens (SENB) 25 mm thick, 50 mm wide, and 255 mm long for measurement of the fracture toughness.

The orientation of all specimens was *L–T*.

Tensile tests were carried out in the temperature range from −196°C to ambient. The SENB specimens were fatigue precracked according to ASTM E-399. The specimens were loaded by three point bending under displacement control. Inductive gauges were used for the measurement of load and crack opening displacement. Static tests were carried out in the temperature range from −170°C to ambient temperature, the stress intensity factor rate ($\dot{K}_I$) in the elastic region being 2 MPa $m^{1/2}$ s^{-1}.

Instrumented impact testing and static testing of Charpy specimens were carried out only in the temperature range in which brittle fracture occurred.

Load/deflection diagrams were recorded during testing. The aim of tests was to estimate the critical tensile stress for brittle fracture initiation.

Results and discussion

Tensile properties

Yield stress R_{eL}, ultimate tensile stress R_m, nominal fracture stress σ_{FR} (fracture load divided by fracture area) and reduction in area RA versus temperature are presented in Fig. 1. The results show that the yield stress R_{eL} and

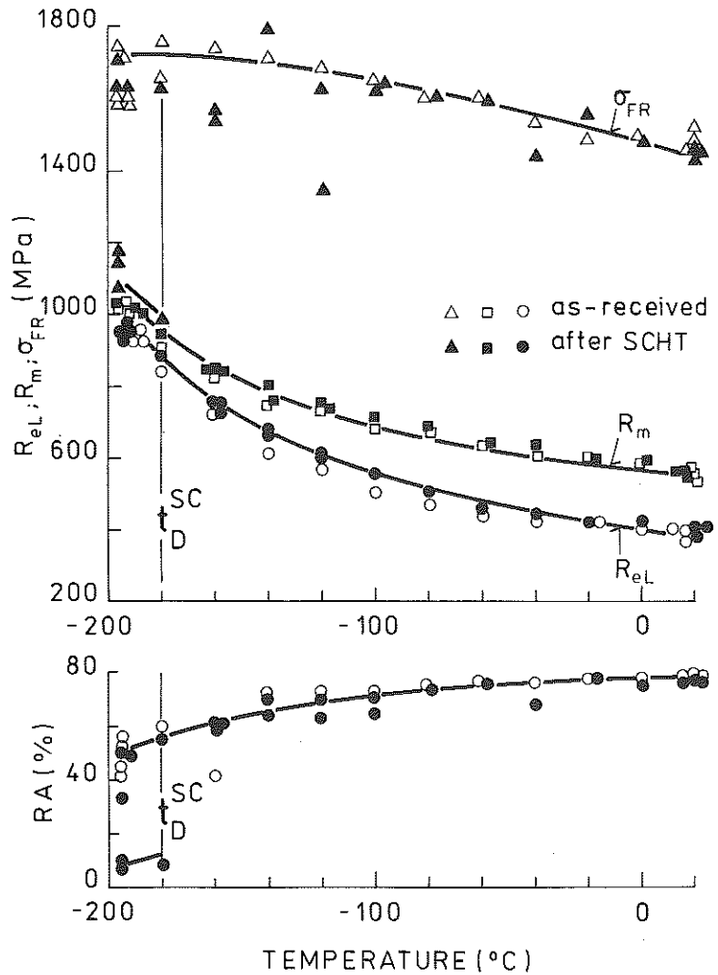

Fig 1 The dependence of yield stress R_{eL}, ultimate tensile stress R_m, fracture stress σ_{FR} and reduction of area RA on temperature

the ultimate tensile stress R_m are not influenced by SCHT and that both tensile characteristics increase with decreasing temperature. This means that the dislocation mechanism controlling yield stress, strain hardening, and the ultimate tensile stress are not influenced by SCHT.

Only ductile failure with high RA values slowly decreasing with decreasing temperature can be observed for the as-received condition. The nominal fracture stress σ_{FR} for this condition increases moderately with decreasing temperature. In the case of the SCHT condition, both the ductile cup-cone failure with a high RA value, and the flat fracture without necking with a low RA value and markedly lower fracture stress can be observed. A temperature of $-180°C$ can be designated as the ductility transition temperature **(21)** for plain tensile specimens of the SCHT condition. These results prove that changes in the structure of a 2.25Cr–1Mo steel occur as a result of SCHT. According to various authors **(4)(12)(22)**, the susceptibility of a given steel to temper embrittlement or to long term temperature embrittlement can be established by SCHT. Embrittlement is caused by the segregation of impurities along grain boundaries followed by intergranular fracture at lower fracture stresses and higher temperatures **(8)(23)**. This was the case for specimens having low values for nominal fracture stress, Fig. 2. However, these results also suggest that some regions of the blanks suffer more embrittlement after SCHT than others, indicating the heterogeneous character of the segregation processes.

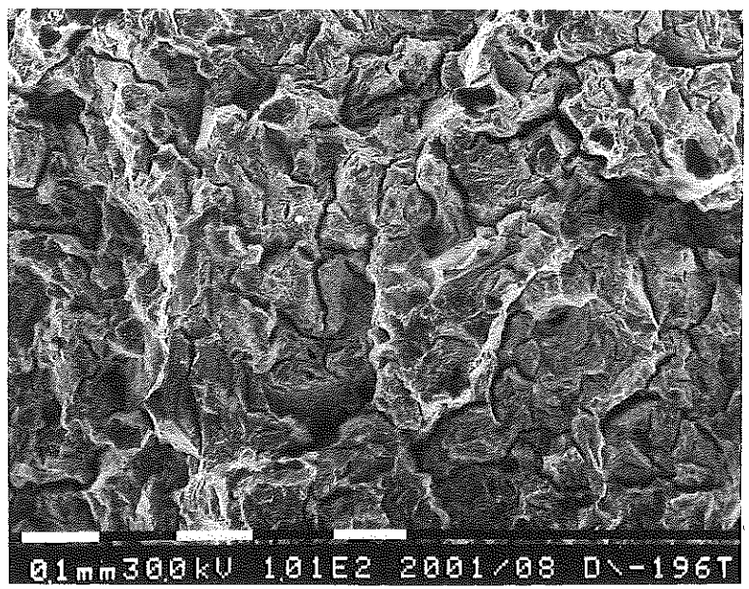

Fig 2 The appearance of the fracture of a SCHT specimen with low nominal fracture stress (testing temperature – 196°C)

Charpy 'V' notch properties – standard testing

The dependence of CVN energy on temperature is presented for the as-received condition in Fig. 3(a) and for the SCHT condition in Fig. 3(b). In the diagrams the fracture appearance (percentage of fibrous fracture) and the length l_s of the ductile crack extension ahead of the notch are also plotted. Although the dependence of the CVN energy on temperature is generally considered to be a continuous curve, often with a large scatter of energy values, for the purposes of evaluating fracture behaviour this method is inadequate. The approach proposed by Teleman and McEvily **(21)** and elaborated by

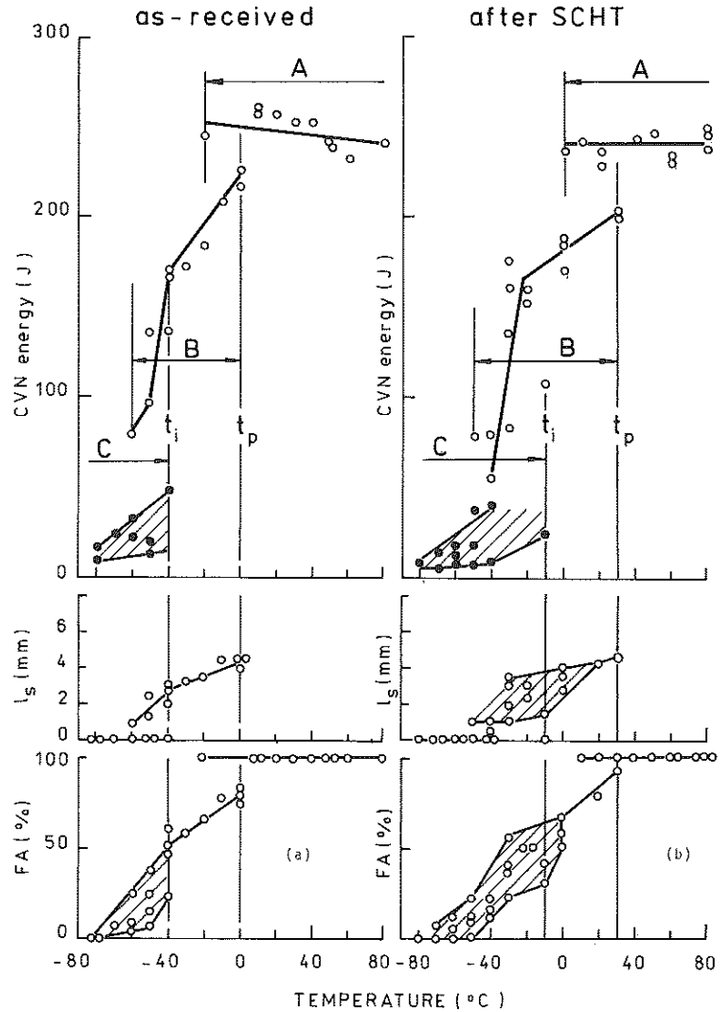

Fig 3 The dependence of CVN energy, ductile crack extension l_s and fracture appearance FA on temperature

Helms *et al.* **(36)** was therefore used in order to study transition behaviour. According to this approach it is possible to define the following transition temperatures in the CVN plot:

t_p– propagation transition temperature, at and below this temperature a change in the crack propagation mechanism occurs, i.e., brittle fracture is initiated after some ductile crack growth;

t_i– initiation transition temperature, at or below this temperature brittle fracture occurs: by cleavage mechanisms in the as-received condition or by mixed-mode mechanisms (intergranular cracking and cleavage) after SCHT.

These temperatures are indicated in Fig. 3. The fracture behaviour of 'V' notched Charpy specimens may be divided by means of these temperatures into three main regions.

Region A–region of ductile initiation and ductile crack growth (upper shelf region).

Region B–ductile initiation, after some ductile crack extension with a transition to brittle fracture. An important fracture parameter is the length of stable ductile crack growth l_s (Fig. 3).

Region C–brittle initiation and propagation (cleavage for as-received state and mixed-mode after SCHT).

The fracture regions are superimposed on each other as a consequence of the intrinsic material property scatter. The temperature t_p was therefore taken as the temperature above which only ductile fracture occurred, and the temperature t_i as the temperature at and below which brittle initiation had already occurred.

The results given in Fig. 3 show that SCHT resulted in the following.

- A shift in the transition temperature t_p and t_i by 30°C to higher temperatures. The shift of FATT is 30°C and is in agreement with the data given by Viswanathan and Jaffe **(19)** for a 2.25Cr–1Mo steel with J factor of 200. At the same time, in the set of specimens after SCHT there are specimens with fracture behaviour identical to that of the as-received specimens.
- A pronounced increase in the scatter of the CVN energy values in the transition range t_p–t_i and the increase of the temperature range in which regions B and C are superimposed: from 20°C in the as-received state to 60°C after SCHT. In this interval the fracture is bimodal.
- In the upper shelf toughness region A, the CVN energy is not influenced by SCHT.

The heterogeneous character of segregation processes is therefore conformed by the Charpy 'V' notch results. When investigating the fracture surface of specimens after SCHT with brittle initation it was found that the fracture surfaces both in the initiation site ahead of the notch and in the area

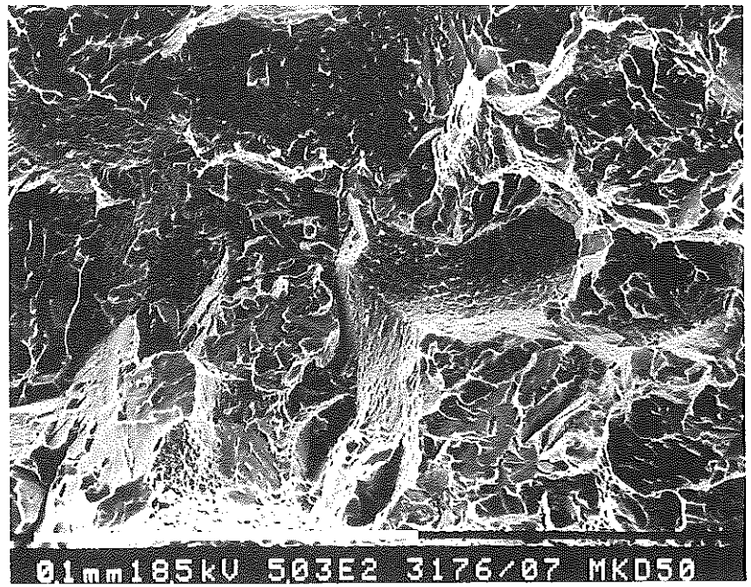

Fig 4 Fracture surface of Charpy specimen after SCHT tested at −50°C

of unstable fracture propagation had a mixed-mode character, i.e., intergranular cracked regions surrounded by transgranular cleavage (Fig. 4). As the variation of principal stress and the maximum value of this stress ahead of the notch are the same for both conditions at any given temperature (yield stress and hardening properties are not influenced by SCHT) and because t_i for SCHT is higher, mixed-mode fracture requires a lower critical tensile stress for brittle fracture initiation. The shift of the transition temperature by SCHT can, therefore, be explained as being due to the presence of locally embrittled regions caused by SCHT.

Critical tensile stress

Using Charpy specimens and instrumented impact testing the load F_{GY} (general yield load) and F_{FR} (fracture load) were measured in Region C (Figs 3, 5, and 6). The point of intersection of the temperature dependence of these loads determines the brittleness transition temperature t_{Bv} at which $F_{GY} = F_{FR}$. At this temperature the Region C is divided into two intervals, C′ and C″. In the range C″, $F_{GY} > F_{FR}$, load deflection dependence is practically linear up to fracture and the fracture time τ_{FR} is very short. In order to measure the true fracture load [fulfilling the condition $\tau_{FR} \geqslant 3\,\tau$, where τ is the period of natural Charpy specimen oscillations **(34)**], impact tests had to be carried out at the lower impact velocity of 1.5 ms^{-1}. The ratio of F_{FR}/F_{GY} in the temperature range C″ makes it possible to determine the critical tensile stress σ_{11} at the

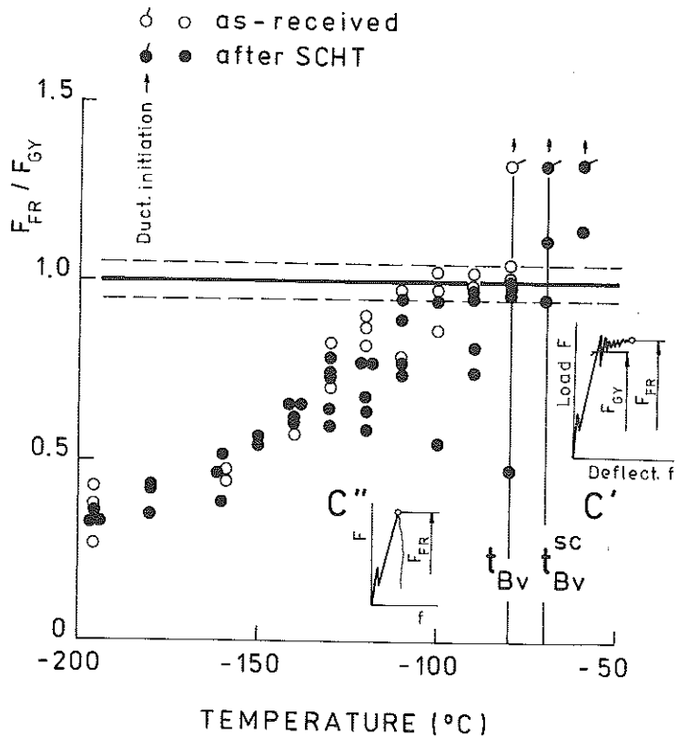

Fig 5 The ratio F_{FR}/F_{GY} versus temperature – impact loading

brittle fracture initiation. In order to verify whether or not the condition of fracture initiation in the interval C″ depends on the loading rate and temperature, Charpy specimens were also loaded statically (deflection rate 0.033 mm s^{-1}), and the temperature dependence of the loads F_{GY} and F_{FR} in the temperature interval C was determined.

In order to determine the maximum value of the maximum principal tensile stress σ_{11}^{max} at brittle fracture initiation in the interval C″ the method described by Wilshaw *et al.* **(24)** was used. According to this method, σ_{11}^{max} is determined by the relation

$$\sigma_{11}^{max} = K_{\sigma p} R_e$$

or

$$\sigma_{11}^{max} = K_{\sigma p} R_e^d,$$

where $K_{\sigma p}$ is the plastic stress concentration factor, being a function of the ratio F_{FR}/F_{GY} as given in the paper mentioned above. The determination of F_{GY} and R_e^d below t_{Bv} has been described in **(25)**. Yield stress R_e at static

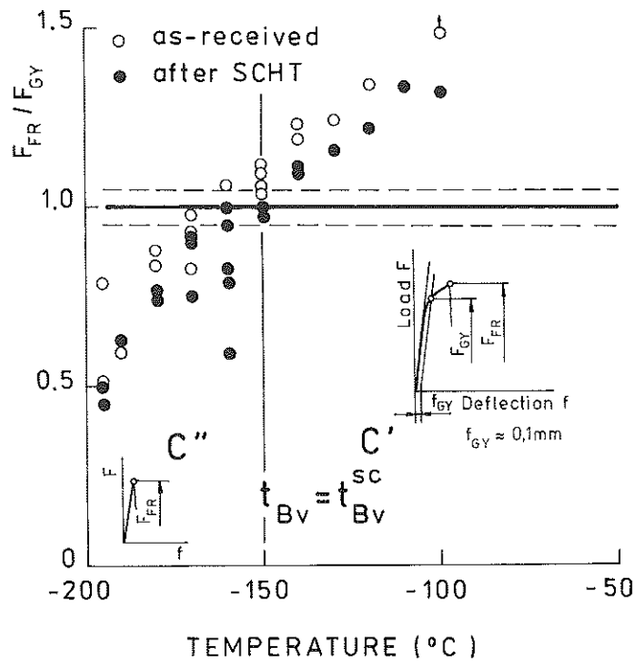

Fig 6 The ratio F_{FR}/F_{GY} versus temperature – static loading

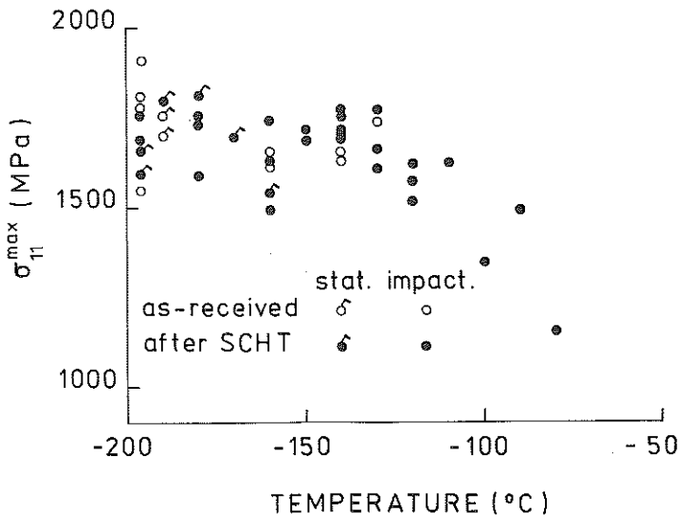

Fig 7 The dependence of the maximum value of the maximum principal stress on temperature

loading was taken from Fig. 1. Dependence of the ratio F_{FR}/F_{GY} on temperature is given for impact loading in Fig. 5 and for static loading in Fig. 6. The transition temperature t_{Bv} is shown in the diagrams; its value is practically unchanged by SCHT.

The calculated values of σ_{11}^{max} depending on temperature are given for both conditions and loading rates in Fig. 7. Disregarding two values of σ_{11}^{max} (temperature $-80°C$ and $-100°C$: their significance is discussed below), it can be shown that σ_{11}^{max} depends neither on temperature nor on loading rate and has, therefore, as a brittle fracture initiation criterion the same meaning as the cleavage fracture stress for initiation of brittle fracture in low carbon steel [Knott **(26)**].

The influence of SCHT on the σ_{11}^{max} values is difficult to estimate due to scatter from the diagram in Fig. 7. In order to compare σ_{11}^{max} values for both conditions and to assess the influence of SCHT on this stress the Weibull distribution was used **(28)**. The cumulative distribution function

$$P = 1 - \exp\left(\frac{\sigma_{11}^{max}}{\sigma_0}\right)^m$$

for the set of measurements is shown in the Weibull probability paper for the as-received condition in Fig. 8(a) and for the SCHT condition in Fig. 8(b). The shape parameter $m = 20.4$ and the scale parameter $\sigma_0 = 1756$ Mpa for as-received state. It can be seen that, for the as-received condition, critical tensile stress perfectly fits a two-parameter Weibull distribution. For the condition after SCHT two straight lines provide a better fit to the experimental results. Splitting in two straight lines indicates double population after SCHT. Even the measured very low values of σ_{11}^{max} (Fig. 7) lie on the straight line 1. Fractographic investigation of the fracture surfaces of specimens on lines 1 and 2, Fig. 8(b), was therefore, carried out. This investigation showed that the fracture surface of a set of specimens from line 2 was 100 percent cleavage, while fracture surfaces of the set of specimens of line 1 was mixed-mode (intergranular cracking surrounded by transgranular cleavage). Due this observation the set of measurements was divided into two populations and for each of them the parameters m and σ_0 were determined. The following values were obtained: for the set of specimens with 100 percent cleavage fracture surfaces $\sigma_0 = 1728$ MPa (practically the same value as in the as-received state) and $m = 35.86$, for the set of specimens with mixed-mode fracture surfaces $\sigma_0 = 1537$ MPa and $m = 9.98$.

The results show that the 2.25Cr–1Mo steel blanks contain, after SCHT, both regions with resistance to brittle fracture initiation, similar to that in the as-received condition and embrittled zones where σ_{11}^{max} for brittle fracture initiation is clearly lower. Low values of σ_{11}^{max} are connected with mixed-mode initiation mechanisms which result from segregation during SCHT. The decrease of fracture stress as a consequence of grain boundary segregation in Cr–Ni steels was measured by Ritchie *et al.* **(23)** and by Kameda and

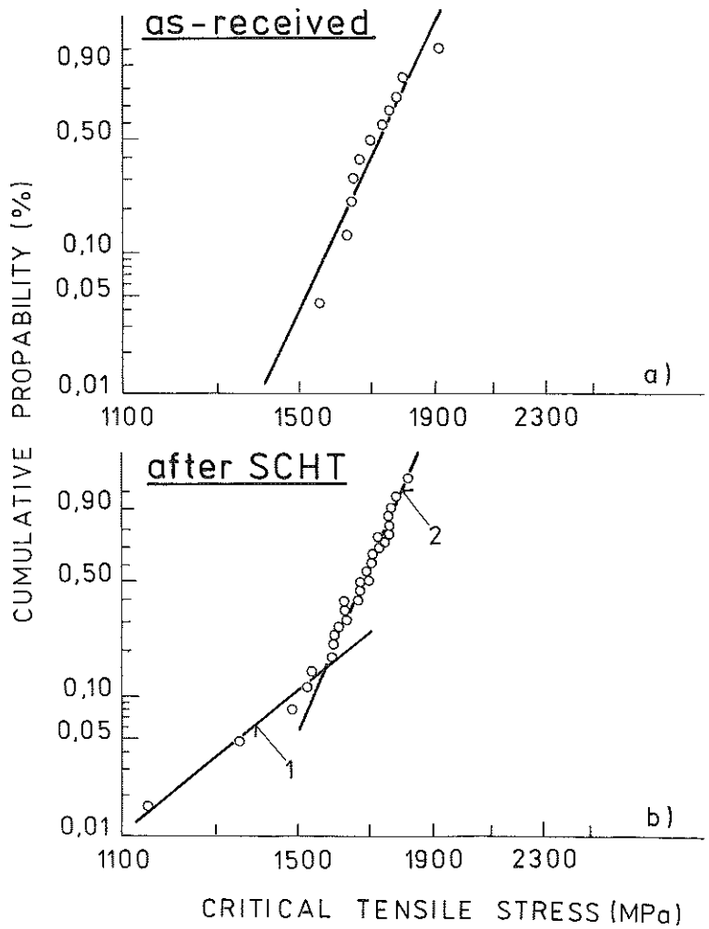

Fig 8 Cumulative probability P versus critical tensile stress σ_{11}^{max}

McMahon **(8)**. According to these authors, this decrease is related to the lowering in intergranular cohesive energy resulting in easier microcrack propagation beyond hard particles on grain boundaries.

Fracture toughness

Fracture toughness versus temperature is plotted for the as-received condition in Fig. 9 and after SCHT, in Fig. 10. The following fracture toughness values are shown:

K_{IC} – measured according to ASTM E 399-83;
$K_{JC} = \sqrt{\{(EJ_c/(1 - \nu^2)\}}$;

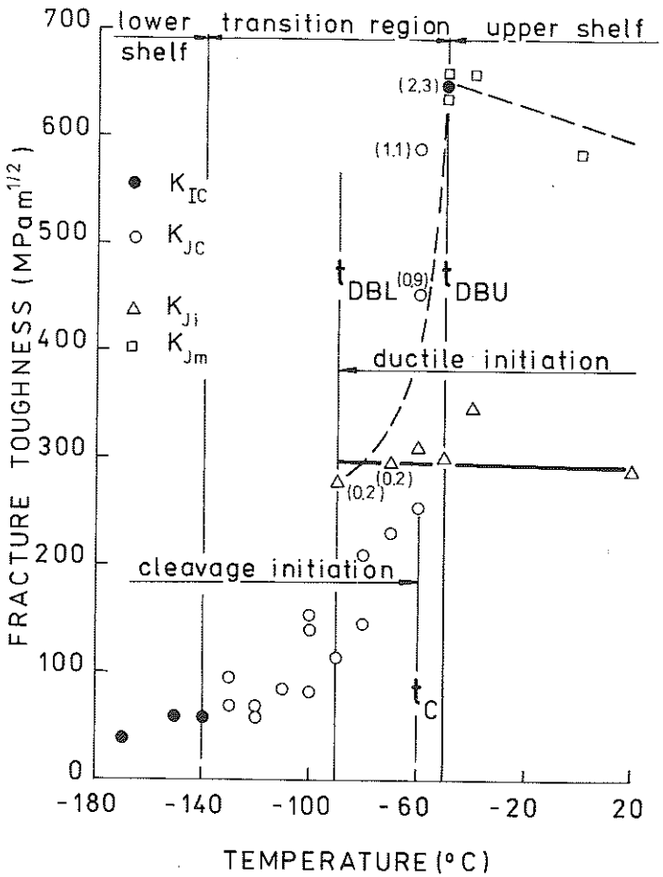

Fig 9 Fracture toughness/temperature dependence – as-received state

The value J_C was determined for the onset of the initiation of unstable brittle fracture. The following relationship was used to calculate J_C **(35)**

$$J_C = J_{CE} + J_{CP} = \frac{1-\nu^2}{E} K_C^2 + \frac{2A_{CP}}{B(W-a)}$$

where

$$K_C = \frac{F_{FR} Y}{B\sqrt{W}}$$

A_{CP} is the plastic work to fracture and F_{FR} is the fracture load.
K_{JCu} is the fracture toughness for unstable brittle fracture after some ductile crack extension (the length of which is labelled in the diagrams).

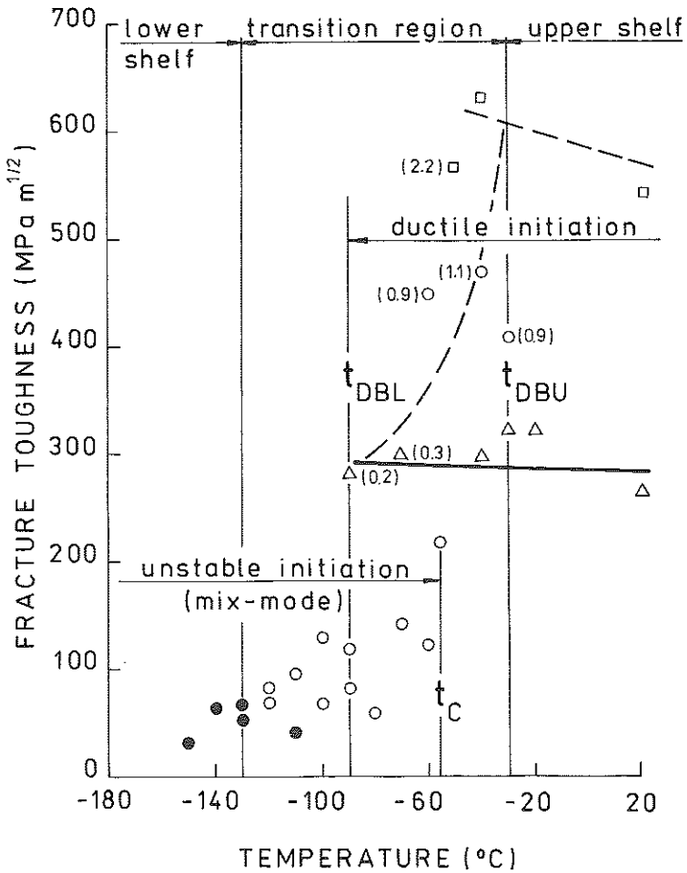

Fig 10 Fracture toughness/temperature dependence after SCHT

K_{Ji} is the fracture toughness for ductile crack initiation measured by the direct current potential drop method.
K_{Jm} is the fracture toughness for maximum load F_{max} in the load/displacement diagram.

The above formula was used for the calculation of K_{JCu}, K_{Ji}, and K_{Jm}.

In order to assess the influence of metallurgical and process variables on fracture toughness and its transition behaviour an exact definition of transition temperature is necessary and the fracture toughness results should be analysed by statistical methods. Having taken into account the results in **(29)**–**(33)** and considering the experimental results obtained with steel used the following transition temperatures are designated in Figs 9 and 10:

t_{DBU}– upper limit of the transition region, below t_{DBU} unstable brittle fracture occurs after some ductile crack growth before reaching F_{max};

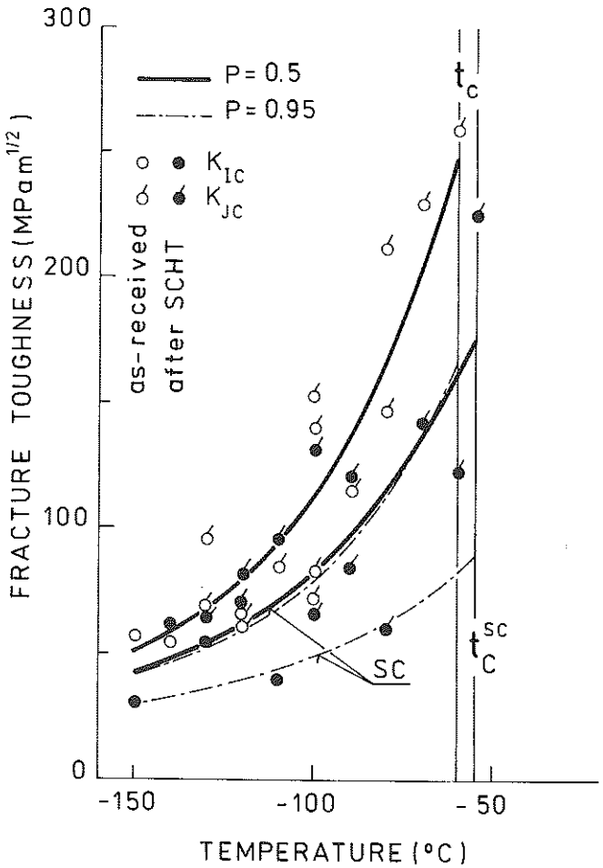

Fig 11 Fracture toughness versus temperature below t_C

t_{DBL} – lower limit of the transition region, in which the above described failure occurs;

t_C – the temperature at and below which elastic–plastic unstable brittle fracture occurs on the blunting line. Due to the scatter this temperature can lie within the range $t_{DBU} - t_{DBL}$;

$t_{2.5}$ – the region of lower shelf fracture toughness values (plane strain fracture toughness for a given specimen thickness) is below this temperature.

The fracture toughness versus temperature curve is divided into three main regions (Figs 9 and 10) as defined above. By comparing the results presented in Figs 9 and 10 the following conclusions can be drawn:

- SCHT does not influence the fracture toughness in the upper shelf region;

- the shift of transition temperature t_{DBU}, t_{DBL}, and t_C by SCHT is only by about 10°C to 15°C. Exact determination of the temperature shift would require the testing of a larger number of specimens;
- the marked influence of SCHT on fracture toughness was observed below temperature t_C. After SCHT fracture toughness was reduced.

In order to compare the fracture toughness temperature dependence for both conditions below temperature t_C the equation

$$K_{IC}, K_{JC} = K_0 + A \exp(BT)$$

was used. Having chosen the constant $K_0 = 25$ MPam$^{1/2}$ the parameters A and B can be calculated by linear regression analysis and the confidence limit for, the linear regression function for any given probability can be calculated. The median fracture toughness curve (P = 50 percent) and the fracture toughness curve for confidence limit P = 95 percent are given for both conditions in Fig. 11. Only the values of K_{JC} for unstable fractures without ductile crack growth were taken for this calculation. It can be seen that, due to SCHT, a decrease in the median value appears but a much larger decrease can be observed for confidence limit P = 95 percent. Both median and lower bound fracture toughness curves are shifted due to SCHT to a higher temperature. However both curves end at the transition temperature t_C^{SC}, which was not much influenced by SCHT.

The investigation of the fracture surface of specimens with a fracture toughness value on the lower bound fracture toughness curve confirmed the presence of mixed-mode fracture.

Conclusions

(1) The tensile properties (yield stress, ultimate tensile stress, reduction in area) in the temperature interval from −170°C to 20°C are not influenced by SCHT. Below a temperature of −170°C the failure of some tensile specimens after SCHT occurs at markedly lower fracture stress and with a low value of reduction in area. This decrease in the properties is caused by the occurrence of mixed-mode fracture (intergranular cracking surrounded by transgranular cleavage facets).

(2) The propagation t_p and the initiation t_i transition temperatures measured with Charpy 'V' notch specimens are shifted, after SCHT, by about 30°C. However, it was found that after SCHT some of the Charpy 'V' notch specimens had the same impact notch properties as in the as-received condition. These results show that the embrittlement, probably caused by impurity segregation, has a pronounced heterogeneous character.

(3) The heterogeneous character of the embrittlement process during SCHT was also confirmed by measurement of the critical tensile stress for brittle fracture initation of 'V' notch specimens. After SCHT cleavage initiation at

critical tensile stress values very similar to those of the as-received condition was observed. Brittle initiation also took place at lower stresses due to mixed-mode failures.

(4) Fracture toughness measurements show that the median and lower bound fracture toughness temperature curves for unstable brittle initiated failures were shifted towards higher temperature due to SCHT. The transition temperature below which this kind of fracture occurred was not influenced by SCHT.

References

(1) COULON, P. A., SAISE, H., and THAUVIN, G. (1983) *J. Testing Evaluation*, **11**, 16–26.
(2) VISWANATHAN, R. and BRUEMMER, S. M. (1985) *J. Engng Mater. Technol.*, **107**, 316–324.
(3) VISWANATHAN, R., BRUEMMER, S. M., and RICHMAN, R. H. (1988) *J. Engng Mater. Technol.*, **110**, 313–318.
(4) CLASS, I. and MILLION, A. (1981) *Oerlikon Schweissmitteilungen Jahrgang*, **39**, Nr. 96/97, 7–13.
(5) LOW, Jr. J. R., STEIN, D. F., and TURKALO, A. M. (1968) Trans *AIME*, **42**, 14–24.
(6) NARAYAN, R. and MURPHY, M. C. (1973) *JISI*, 493–501.
(7) *Temper Embrittlement of Alloy Steels* (1972) *STP* **499** ASTM, Philadelphia.
(8) KAMEDA, J. and McMAHON Jr., C. J. (1980) *Met. Trans*, **11A**, 91–101.
(9) POWER, A. E. (1956) *Trans ASM* **48**, 149–164.
(10) SUZUKI, M., FUKAYA, K., KOIDARA, T., and OKU, T. (1984) *Intern. Conf. on Pressure Vessel Technology, San Francisco*, Vol. II, ASME Publication, pp. 891–904.
(11) DRUCE, S. G., GAGE, G. and JORDAN, G. (1986) *Acta Met.*, **34**, 641–652.
(12) GROSSE-WOERDERMANN, J. and DITTRICH, S. (1982) *Met. Progress*, **122**, 43–49.
(13) JIN YU and McMAHON Jr., C. J. (1980) *Met. Trans*, **11A**, 277–289; 291–303.
(14) ASTAJEV, A. A., JUCHAMOV, V. A., SUR, A. D., and BOBKOV, K. V. (1984) *Zavodskaja Laboratorija Tom 50*, **10**, 57–64 (in Russian).
(15) HUDSON, J., DRUCE, S. G., GAGE, G., and WALL, M. (1986) IAEA Specialist's Meeting on: Load and Time Dependent Material Performance other than Irradiation, Budapest.
(16) VISWANATHAN, R. (1979) MiCon 78: Optimalization of processing properties and service performance through microstructural control *ASTM STP* **672**, pp. 169–185.
(17) Characterisation study of temper embrittlement of chromium–molybdenum steels (1982) *API Publication 959*, American Petroleum Institut, Washington.
(18) SWIFT, R. A. and GULYA, J. A. (1973) *Welding Res. Suppl.*, **52**, 57–68.
(19) VISWANATHAN, R. and JAFFE, R. I. (1982) *J. Eng. Mater. Technol.*, **104**, 220–226.
(20) IWADATE, T., KARAUSHI, T., and WATANABE, J. (1979) Fracture Mechanics of Ductile and Tough Materials and its Application to Energy Related Structures Proceedings, *USA – Japan sem., Hyama Japan* (Edited by H. W. Liu, T. Kunio, V. Weiss, and H. Okumura), Martinus Nijhoff, The Netherlands.
(21) TETELMAN, S. and McEVILY Jr., A. J. (1967) *Fracture of Structural Materials*, John Wiley, New York.
(22) PRESCOTT, G. R. (1981) *Met. Progress*, **120**, 24–30.
(23) RITCHIE, R. O., GENIETS, L. C. E. and KNOTT, J. (1973) *Proceed. Third Intern. Conf. on the Strength of Metals and Alloys*, Vol. I, pp. 124–128.
(24) WILSHAW, T. R., RAU, C. A., and TETELMAN, A. S. (1986) *Engng Fracture Mech.*, **1**, 191–211.
(25) HOLZMANN, M., VLACH, B., and MAN, J. (1986) *ECF 6, Fract. Control of Eng. Structures*, **III**, (Edited by H. C. van Elst and A. Bakker), EMAS, pp. 1705–1720.
(26) KNOTT, J. F. (1973) *Fundamentals of Fract. Mech.*, Butterworths, London.
(27) IWADATE, T., WATANABE, J., and TANAKA, Y. (1985) *J. Pressure Vessel Technol.*, **107**, 230–238.
(28) WEIBULL, W. (1951) *J. Appl. Mech.*, 293–297.

(29) MILNE, I. and CURRY, D. A. Elastic–plastic fracture, Second Symp. *ASTM STP 803*, Vol. **II**, pp. II-278–II-290.
(30) DAWES, M. G. Elastic–plastic fracture, Test Methods, *ASTM STP 856*, pp. 258–264.
(31) IWADATE, T., TANAKA, Y., ONO, S. I., and WATANABE, J. Elastic–plastic fracture, Second Symp. *ASTM STP 803*, Vol. II, pp. II-531–II-561.
(32) WATANABE, J., IWADATE, T., TANAKA, Y., YOKOBORI, T., and ANDO, K. (1987) *Engng Fracture Mech.*, **28**, 589–600.
(33) LIDBURRY, D. P. G. and MORLAND, E. (1987) *Int. J. Pressure Vessels Piping*, **29**, 343–428.
(34) SERWER, W. L. (1987) *J. Testing Evaluation*, **6**, 29–34.
(35) SUMPTER, D. C. and TURNER, C. E. (1976) Cracks and fracture, *ASTM STP 601*, pp. 3–18.
(36) HELMS, R., KUHN, H. J., and LEDWORUSKI, S. (1982) *Forschungsbericht* **82**, Bundesanstalt für Materialprüfung, Berling.